Detecting extra-galactic supernova neutrinos in the Antarctic ice

Sebastian Böser*, Marek Kowalski, Lukas Schulte, Nora Linn Strotjohann, Markus Voge

Physikalisches Institut, Universität Bonn, D-53115 Bonn, Germany

Abstract

Building on the technological success of the IceCube neutrino telescope, we outline a prospective low-energy extension that utilizes the clear ice of the South Pole. Aiming at a 10 Mton effective volume and a 10 MeV threshold, the detector would provide sufficient sensitivity to detect neutrino bursts from core-collapse supernovae (SNe) in nearby galaxies. The detector geometry and required density of instrumentation are discussed along with the requirements to control the various sources of background. We find that the resulting detector will be able to detect SNe from beyond 10 Mpc, delivering between 11 and 46 regular core-collapse SN detections per decade. It would further allow to study more speculative phenomena, such as optically dark (failed) SNe, where the collapse proceeds directly to a black hole, at a detection rate similar to the regular SNe. We find that the biggest technological challenge lies in the required large number of large area photo-sensors, with simultaneous strict limits on the allowed noise rates. If both can be realized, the detector concept we present will reach the required sensitivity in a cost effective manner and hence offers a route to future routine observations of SNe with neutrinos.

Keywords: supernovae, core-collapse, neutrino physics, neutrino detectors

1. Introduction

In 1987, Supernova 1987A (SN 1987A) exploded in the Large Magellanic Cloud at a distance of only 50 kpc, leading to the first detection of neutrinos from outside our solar system. Despite the fact that only ∼20 supernova neutrinos were detected in total [1], a wealth of papers has been published in its wake (see e.g. [2] for a summary), reflecting the numerous and fundamental roles that neutrinos play in astrophysics as well as in particle physics (e.g. see [3, 4]).

Given today's detectors, a supernova in our Galaxy would result in $\sim 10^4$ neutrino events detected individually in Super-Kamiokande [5] and other large low-energy neutrino detectors, as well as up to millions of neutrinos detected through an increase in noise rate in IceCube [6]. However, with an expected rate of only 1-3 Galactic SNe per century [7, 8], the chance for a detection during the lifetime of the experiments is not overwhelmingly large. In the fortunate case of a SN detection, the uniqueness of the progenitor system will make it difficult to disentangle the astrophysical diversity from the effects due to particle physics (e.g. neutrino oscillations) that will impact the light curve and energy spectra.

As pointed out in [7] and [8], the situation will change drastically once neutrino detectors reach the sensitivity threshold to detect "mini-bursts" of neutrinos from supernovae in neighboring galaxies. Not bound to our own Galaxy, the rate of SN observations will depend only on the size of the detectors. As we will show in section 5, an effective volume of ~ 10 Mtons is sufficient to detect SNe at a rate of $\sim 1-4$ per year—albeit most of them with less than ten individual neutrino events. Despite the low number of detected neutrinos, these routine observations would provide a wealth of information and allow entirely new studies [8]. What follows is a brief and incomplete summary of the scientific benefits of a large supernova neutrino detector.

The total SN rate in our local universe would be determined in a novel and less biased way. Given an apparent mismatch in rates—only about half the expected rate of SNe is actually detected by optical surveys [9]—a direct measurement would hence allow to solve the riddle of missing supernovae.

Furthermore, a significantly sensitive detector allows to test models predicting additional neutrino bursts, such as failed or *dark* (i.e. optically unobservable) SNe [10], merger of binary neutron stars [11] or the formation of quark stars [12]. Dark SNe are core-collapse objects that directly form a black hole (BH). Electromagnetic radiation is strongly suppressed, since the photons don't have time to escape and are swallowed by the forming BH. Neutrinos, on the other hand, can escape, and the expected burst from such an event is both more luminous and hotter [10]. Average neutrino energies can be roughly twice as large as in the case of the collapse to a neutron star (NS) and hence open the opportunity to identify the collapse to a BH. Another opportunity is the identification of questionable SN candidates, e.g. luminous blue variables [13], as "supernova impostors" by the non-detection of neutrinos [8].

*Email: sboeser@physik.uni-bonn.de

In addition, detections of neutrino bursts can be used to trigger early optical or X-ray observations. Having a precise timing for the moment of explosion and observing the shock-breakout in electromagnetic radiation, will allow to infer a wealth of information about the progenitor system. In the absence of a direction for the SN, the follow-up could focus on observation of nearest galaxies, since these are the only ones for which a neutrino detection is expected.

With a larger number of supernova neutrinos, even a broader physics program can be accessed. Due to the complexity of the involved processes, modeling of supernova explosions is still a challenge today and has significant variance in e.g. the predicted mean neutrino energy [14]. Determination of the neutrino luminosity and energy spectrum will provide valuable input to these models.

From the observation of the arrival times of the neutrinos from SN 1987A, a limit of $m_\nu < 5.8\,\mathrm{eV}$ has been set on the mass of the electron neutrino [15]. By observing neutrinos from supernovae with higher statistics, more stringent limits could be set. In addition, by its impact on the predicted flux, the mass hierarchy can be addressed as well, provided a sufficient number of neutrinos is observed [6].

Motivated by this scientific potential, several megaton scale neutrino detectors are currently planned (e.g. Deep-TITAND [8], Hyper-Kamiokande [16, 17] and UNO [18]). Those are either water Cherenkov detectors located in mines or marine detectors, similar to ANTARES. In this paper, we explore the potential of a $\sim 10\,\mathrm{Mton}$ detector in the Antarctic ice shield. In the existing IceCube detector that has been optimized for TeV-PeV energies [19], SN neutrino bursts are typically searched for by looking for a collective enhancement of photomultiplier noise rates [6]. Due to the large sensor spacing and consequently high energy threshold, attempting to detect individual neutrino events in this configuration significantly reduces the effective mass and hence distance at which SNe can be detected [20]. A dedicated effort is now under way to reduce the energy threshold to a few GeV in the PINGU (Phased IceCube Next-Generation Upgrade) project [21], with one of its goals being the determination of the neutrino mass hierarchy through the MSW effect [22]. Building on this effort and the expertise accumulated with IceCube and AMANDA, we explore the capabilities of a dedicated low-energy extension to study individual supernova neutrino events. The challenge is to reduce the energy threshold of the experiment by three orders of magnitude while controlling the background at a level required for the detection of supernovae.

While we will focus on this aspect in this paper, it should be noted that such a detector will not be limited to the detection of neutrinos at a few MeV, but will also provide unprecedented sensitivity at the GeV-scale. Not only the neutrino oscillation sector will be accessible with increased precision — it will also provide sensitivity to other astrophysical phenomena such as collisional heating in gamma-ray bursts [23, 24].

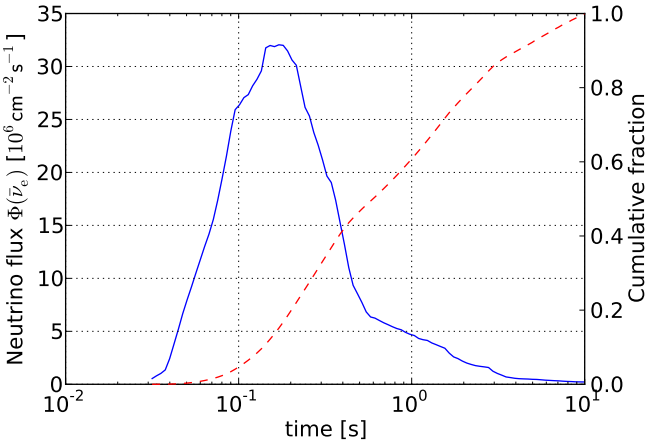

Figure 1: Time evolution of $\bar{\nu}_e$ flux for a SN at 1 Mpc in the Lawrence-Livermore model [26] (full line represents the differential flux and dashed line the integral).

The paper is organized as follows: The SN models that we use to benchmark a future detector are discussed in section 2, followed by a description of our detector simulation and the optimization of the detector configuration in section 3. Section 4 is a discussion of the various background sources that can be anticipated. Finally, we give an estimate on the expected SN rate in section 5 and conclude with a discussion of the results in section 6.

2. Neutrinos from core-collapse supernovae

In core-collapse supernovae, neutrinos are produced in course of the formation of a neutron star which follows the gravitational collapse of a massive progenitor star. Electrons and protons rapidly fuse to neutrons, emitting electron neutrinos, which results in a sharp ($\sim 10\,\mathrm{ms}$) deleptonization peak in the neutrino flux which marks the birth of the neutron star. However, most supernova neutrinos ($\sim 90\%$) originate from thermal pair creation [25]. These neutrinos, released over a characteristic diffusion time of 1-10 s (cf. Fig. 1), are of all flavors, with flavor ratios, light curve and energy spectrum still being under debate [14].

An early simulation of neutrino production in SN explosions has been provided in the so-called Lawrence Livermore (LL) model [26]. In the LL model, the neutrino spectrum is parametrized by

$$\frac{dN}{dE} = \frac{(1+\beta)^{1+\beta} L}{\Gamma(1+\beta)\langle E\rangle^2} \left(\frac{E}{\langle E\rangle}\right)^{\beta} \exp\left(-(1+\beta)\frac{E}{\langle E\rangle}\right), \quad (1)$$

where L is the luminosity and $\langle E\rangle$ the average energy while β determines the width of the spectrum. The parameters for the LL simulation as well as for a competing model by

	Mass $[M_\odot]$	$\langle E_{\overline{\nu}_e} \rangle$ [MeV]	$\beta_{\overline{\nu}_e}$	$L_{\overline{\nu}_e}$ [erg]
LL SN	20	15.4	3.8	$4.9 \cdot 10^{52}$
TBP SN	11 and 15	11.4	3.7	$(4.9 \cdot 10^{52})$
Dark SN	$25 - 40$	$20 - 24$	-	$\sim 10^{53}$

Table 1: Parameters of the Lawrence Livermore (LL) model [2], the Thompson, Burrows, Pinto (TBP) model [27] and the dark supernova model [10] for the neutrino spectrum of a core-collapse supernova. The table presents the stellar mass of the progenitor $M_\odot$, the average neutrino energy $\langle E_{\overline{\nu}_e} \rangle$, the pinch parameter $\beta_{\overline{\nu}_e}$ (see Eqn. 1) and the time-integrated luminosity in anti-electron neutrinos $L_{\overline{\nu}_e}$. The TBP model does not lead to an explosion, i.e. no luminosity emerges from the simulation. Instead, the luminosity from the LL model is assumed. Please note that for dark SNe Eqn. 1 is not valid, instead the positron spectrum given in [10] was used.

Thompson, Burrows and Pinto (TBP) [27] are reproduced in Table 1. While the latter model does not result in an explosion of the supernova, [14] suggests that the resulting luminosity should be of the same order of magnitude. A large variety of other neutrino emission models exists [28], but we restrict ourselves to these two commonly used ones for ease of comparison. Alternative models predicting low-energy neutrinos include *dark supernova models* in which stars heavier than $\sim 25\,\mathrm{M}_\odot$ form black holes. It is assumed that if the black hole rotates fast enough, it explodes as a hypernova, otherwise the event should be very faint or even dark in optical emission, while even more luminous in neutrino flux than ordinary supernovae [29, 30]. The resulting neutrinos have average energies of $\langle E_\nu \rangle \sim 20 - 24\,\mathrm{MeV}$ [10].

The neutrinos from the different collapse scenarios can best be detected via inverse beta decay

$$\overline{\nu}_e + p \rightarrow e^+ + n \qquad (2)$$

that requires a threshold energy of $E_\nu > 1.806\,\mathrm{MeV}$. We use the approximation for the energy dependence of the cross-section called "Naïve +", which is presented in [31]. Since the cross-section rises with energy, the resulting positron spectrum is harder than the initial neutrino spectrum. Figure 2 shows the resulting positron spectra for the two different supernova models as well as for a model of dark supernovae. Neutrino oscillations, which harden the spectrum, are taken into account only for the dark model, for which we directly take the positron spectrum from [10].

For a typical positron energy of 20 MeV the corresponding track length is $\sim 10\,\mathrm{cm}$, resulting in ~ 3600 Cherenkov photons [6]. Since the light yield scales linearly with the positron track length, and hence with the positron energy, the average amount of light produced per neutrino is model dependent.

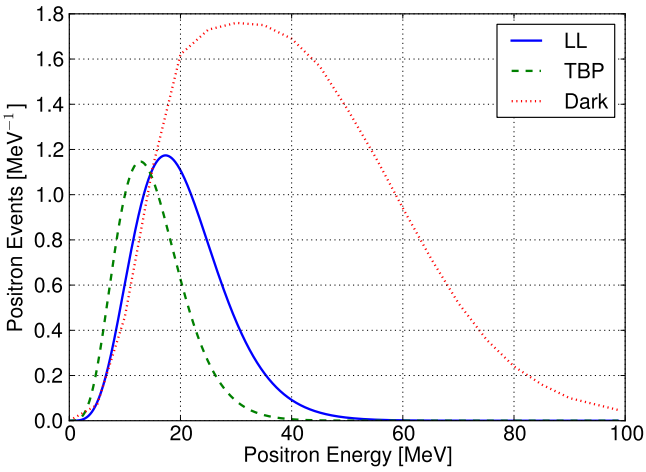

Figure 2: Positron spectrum for the Lawrence-Livermore (LL) [26], Thompson, Burrows, Pinto (TBP) [27] and a dark supernova model [10] for a SN at 1 Mpc and an effective detector volume of 1 Mton.

3. Detector simulation and optimization

In this section we describe the simulation and optimization of a possible detector in the Antarctic ice capable of detecting MeV neutrinos with high statistics. Being embedded in natural ice, special attention has to be given to the optical properties of the detection medium and hence the location of the detector. Two parameters affect the propagation of the Cherenkov light – the absorption length λ_a and the effective scattering length λ_e. Both parameters have been subject to dedicated measurement campaigns during the installation of the AMANDA and IceCube detectors [32–34]. From these measurements, two natural choices for a location of the detector arise:

1. $750 - 1050\,\mathrm{m}$ where the AMANDA-A [35] detector is located. We will call this **diffusive ice**.
2. $2150 - 2450\,\mathrm{m}$ where the DeepCore array is located. We will call this **clear ice**.

In the diffusive ice in a depth range around 900 m, the absorption length of up to $\lambda_a \approx 350\,\mathrm{m}$ is exceptionally large. However, the presence of air bubbles results in very strong scattering with a scattering length of only $\lambda_e \approx 0.3\,\mathrm{m}$ [36]. This results in an effective propagation length of $\lambda_p = \sqrt{\frac{\lambda_e \cdot \lambda_a}{3}} \sim 6\,\mathrm{m}$ after which the photon flux has dropped by a factor e^{-1} [32]. While the photons cannot travel large distances, they are confined within a small volume for a rather long time of $\lambda_a / c \approx 1\,\mu\mathrm{s}$ before finally being absorbed. This leads to a large detection probability, as long as the light is emitted in the vicinity of a photo-sensor. In the diffusive ice the light propagation is well described analytically as a random walk with absorption [32], allowing for convenient simulation of the photon tracking.

Much larger scattering lengths of $\lambda_e \approx 20 - 50\,\mathrm{m}$ are found in the clear ice, at depth $\sim 2300\,\mathrm{m}$, where air bubbles have fully degenerated due to the high ambient pressure and only a small dust concentration was measured. The absorption length in this clear ice is $\lambda_a \approx 20 - 90\,\mathrm{m}$, depending on wavelength [33, 34], providing a good environment for a neutrino detector. In particular, the large scattering length allows for precise reconstruction of the event position and direction. However, compared to diffusive ice, the photons are more likely to travel through the ice without hitting a photo-sensor. For the clear ice, the *Photonics code* [37–39]—a Monte Carlo simulation developed for IceCube—is employed for accurate simulation of the photon propagation. It includes the full depth dependence of the scattering and absorption properties of the ice [33].

In what follows, detectors in both depths will be discussed. We will show that in a pure photon counting argument the diffusive ice is superior to the clear ice. However, the possibility to reconstruct individual events in the clear ice will allow to address a broader spectrum of physics questions. Also in terms of background, the diffusive ice is disfavored. In the clear ice, the atmospheric muon flux is greatly suppressed due to the large overburden and our studies show that reconstruction of neutrino direction – impossible in the diffusive ice – will be important for discrimination of solar neutrinos. We will also show that reconstruction of the neutrino events is required to overcome the large background from self-noise in the photo-sensors. Hence, the clear ice is the preferred location.

In these first simulations, each of the detectors is assumed to consist of 61 strings of 300 m length, with one photo-sensor per meter. In order to get a fairly homogenous distribution of sensors in the ice, the strings are arranged in a filled hexagon, similar to the layout of the IceCube detector. For the diffusive ice, we model the photo-sensors as vertically aligned tubes of 100% efficiency with $l = 1\,\mathrm{m}$ length and $\pi \cdot d = 1\,\mathrm{cm}$ circumference. Averaging over all directions and considering projectional effects, the cylindrical sensor has an effective area of $\langle A_{\mathrm{eff}} \rangle = \frac{\pi}{4} \cdot l \cdot d = 25\,\mathrm{cm}^2$. For the simulation of the clear ice, we assume IceCube-like photo-sensors, i.e. the so-called digital optical module (DOM) [40]. Each DOM includes a 10" Hamamatsu PMT, which is integrated into a pressure resistant glass sphere that also includes the electronics for HV generation and in-ice digitalization of the PMT signal. IceCube employs both regular efficiency and high-quantum efficiency (HQE) PMTs. The dark noise rate of individual DOMs averages around 500 Hz [6]. IceCube DOMs have a non-trivial directional sensitivity [41] which is incorporated in the Photonics simulation package [39] and hence included in our simulation. From laboratory measurements [42], we obtain a Cherenkov-weighted effective area of 19.4 (26.3) cm^2 for an IceCube DOM equipped with a regular (HQE) PMT. In order to achieve a comparable

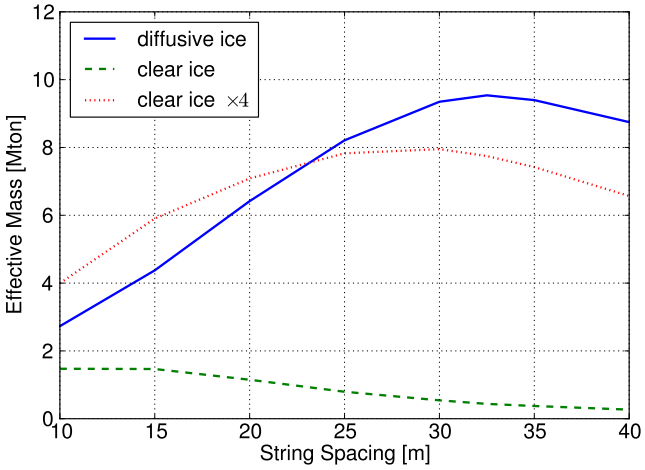

Figure 3: The effective detector mass at trigger level for a 61-string geometry (averaged over the LL model spectrum) as function of string spacing. In clear ice (dashed) the effective mass is several times lower than in diffusive ice (solid) due to ice properties. Only if the sensor effective area is increased by a factor of four (dotted), similar results can be obtained.

detector sensitivity in the clear and diffusive ice, we find that we need to boost the photo-sensitive area for the detectors in clear ice. We therefore scale the sensor response for the DOMs we simulate in the clear ice to obtain effective areas of $35.6\,\mathrm{cm}^2$ and $4 \times 35.6\,\mathrm{cm}^2$ per meter of instrumented string.

In order to optimize the detector geometry, the effective neutrino detection volume is calculated as function of the lateral spacing between strings. We employ a Monte Carlo method where neutrino vertices are generated homogeneously within and beyond the detector volume. The positron energy is sampled according to the respective energy spectrum shown in Fig. 2. The average number of detected photons is calculated for each sensor with respect to the neutrino vertex. For the diffusive ice, this is done via analytic functions, for the clear ice, the Photonics code is employed. The actual number of detected photons is drawn from a Poisson distribution and the arrival times are sampled for each of these photons from the respective arrival time distribution.

We then calculate the *effective mass*, i.e. the mass of the geometrical simulation volume multiplied with the fraction of neutrinos that are detected above threshold. This threshold is set at a minimum of five photo-sensors being hit by photons. The threshold of five sensors is chosen to allow reconstruction of the vertex position and positron direction which add five degrees of freedom. Figure 3 shows the resulting effective mass as a function of the string spacing for the clear and diffusive ice. Generally one finds that, as the string distance increases, the geometri-

cal detector volume increases as well, but the fraction of detected neutrino events with at least five hit sensors decreases, yielding a maximum effective volume for a string spacing around 30 m for a Lawrence-Livermore neutrino spectrum. The maximum effective mass at trigger level in the diffusive ice is $\approx 9.5\,\mathrm{Mton}$. In the clear ice, a much smaller effective mass of $\approx 1.5\,\mathrm{Mton}$ is achieved using the same effective photo-sensitive sensor area as in the diffusive ice. In order to achieve the goal of a close to 10 Mton detector, we increase the sensor area by a factor four to arrive at a maximized effective mass of $\approx 8\,\mathrm{Mton}$ in the clear ice.

We have also considered an alternative cylindrical detector layout similar to the Super-Kamiokande [5] or Hyper-Kamiokande [16, 17] layouts by simulating a detector that consists of only one ring of strings. The strings form a cylindrical wall that encompasses an un-instrumented volume. However, after optimizing the ring radius for the same number of sensors and strings, we generally find an effective volume that is reduced by 45% compared to the filled hexagonal geometry. This is mainly because the cylinder is open at the top and bottom so that many events are lost. Deploying a horizontal layer of sensor in the antarctic ice is not possible in a cost-efficient manner. Hence, we do not explore the cylindrical geometry any further.

4. Background studies

Up to this point, we have solely implied the trigger requirement—that the number of sensors hit by photons be at least five for each neutrino event. In this section, we will discuss the dominant sources of background and how they can be controlled by implying additional constraints on the distribution of photon hits. Contributions from random noise, atmospheric neutrinos, atmospheric muons and solar neutrinos are considered.

Neutrinos from SNe come in bursts. To be distinguished from uncorrelated background or noise triggers, a SN will need to produce a certain multiplicity of neutrino triggers within a given time window. To estimate the allowed background trigger rate, we assume that a supernova detection can be claimed if three or more events occur within a time window of $\Delta t_{SN} \sim 1 - 10\,\mathrm{s}$. The rate of background triggers that we can allow in order to expect not more than one fake supernova claim per year is

$$\begin{aligned} f_{\max}^{\mathrm{BG}} &\approx \left(\Delta t_{SN}^2 \cdot \frac{1\,\mathrm{yr}}{2}\right)^{-1/3} \\ &= \begin{cases} 3.99\,\mathrm{mHz} & \text{for } \Delta t_{SN} = 1\,\mathrm{s} \\ 0.86\,\mathrm{mHz} & \text{for } \Delta t_{SN} = 10\,\mathrm{s} \end{cases} \end{aligned} \tag{3}$$

Hence, a background trigger rate of at most a few mHz is allowed if one wants to effectively detect SNe via the outburst of neutrinos.

4.1. Sensor noise

Since the Antarctic ice shield is a very low-radioactivity environment, the main sources of random noise are introduced by the detector itself: radioactive isotopes and thermal noise in the photo-sensors and electronics. For the IceCube modules, this results in a dark count rate of $\sim 500\,\mathrm{Hz}$ [6]. While it is known that some fraction of the noise is not purely random, but correlated in time, we will neglect this for simplicity of the discussion presented here. As was shown above, the effective photosensitive area will have to be increased to about $0.014\,\mathrm{m}^2$ per instrumented meter to achieve the effective target mass of 10 Mtons. While conventional PMTs of this size are available, the required thickness of a glass pressure vessel of this size and the cost to drill holes of the corresponding diameters make this option very unattractive. New photo-sensor technologies (e.g. based on wavelength shifters as light collectors) are currently discussed for deployment in future extensions to IceCube, that offer to increase the effective photo-sensitive area while simultaneously significantly reducing the noise rate. These technologies are still in the design phase, so we use dark noise values of 500 Hz, 50 Hz and 10 Hz as templates in absence of a measurement.

As shown above (Eqn. 3), the rate f_{noise} of fake neutrino triggers caused by random noise hits has to be below $\approx 1\,\mathrm{mHz}$ if only one fake supernova event is tolerated per year. We will now calculate this noise trigger rate depending on the total number of modules in the detector N_{tot}, the random noise rate per module f_m, the number of hit modules n_{trig} that is required for a neutrino event to trigger and the trigger time window t_{trig}. Assuming that one module has registered a random noise hit and opened the trigger window, the probability P_m for any module to also see at least one noise hit during this time window t_{trig} is complementary to the probability to register no hit, which can be calculated according to a Poisson distribution

$$P_m = 1 - e^{-f_m \cdot t_{\mathrm{trig}}}. \tag{4}$$

The probability for a noise event P_{noise} is the probability that at least $n_{\mathrm{trig}} - 1$ more modules also encounter a noise hit in the time window. It can be calculated with the binomial distribution, again via the complementary probability of registering less than $n_{\mathrm{trig}} - 2$ noise hits:

$$P_{\mathrm{noise}} = 1 - B_{\mathrm{cum}}(n_{\mathrm{trig}} - 2 \,|\, N_{\mathrm{tot}}, P_m)\ , \tag{5}$$

where $B_{\mathrm{cum}}(m \,|\, n, p) = \sum_{k=0}^{m} \binom{n}{k}\, p^k\, (1-p)^{n-k}$ is the cumulative binomial probability for up to m successes out of n tries with probability p. Apart from boundary effects, the rate of noise triggers in the detector is then

$$f_{\mathrm{noise}} = P_{\mathrm{noise}} \cdot f_m \cdot N_{\mathrm{tot}}. \tag{6}$$

Using generic values for the dark count $f_m = 500\,\mathrm{Hz}$, $N_{\mathrm{tot}} = 18300$ for a detector with 61 strings and 300 modules per string and requiring $n_{\mathrm{trig}} = 5$ hits in $t_{\mathrm{trig}} = 1000\,\mathrm{ns}$ the rate of fake SN events is $f_{\mathrm{noise}} = 9\,\mathrm{MHz}$, i.e.

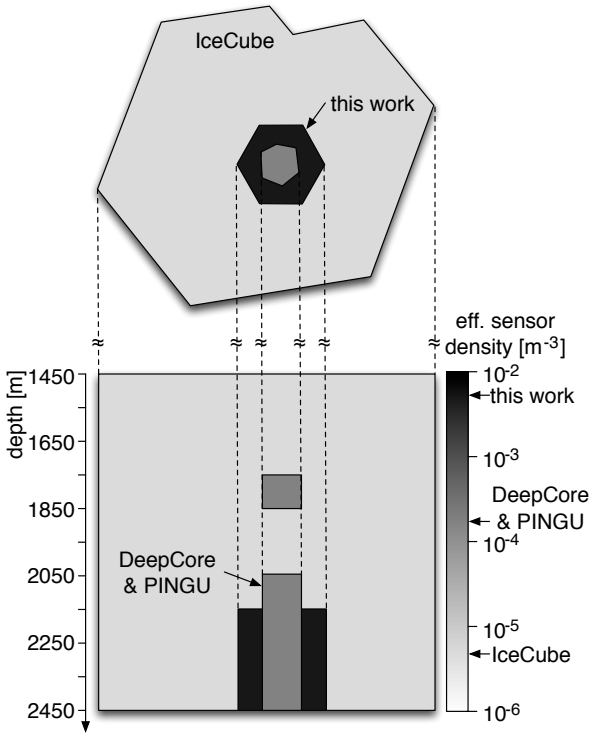

Figure 4: Dimensions and effective sensor density of the final detector layout in the clear ice with 127 strings and 25 m string spacing as compared to the IceCube and PINGU/DeepCore.

is 9 orders of magnitude above the allowed value from Eqn. 3. Even assuming a module dark noise rate as low as $f_m = 10\,\mathrm{Hz}$, still $f_{\mathrm{noise}} = 7.4\,\mathrm{Hz}$, well in excess of what can be tolerated. This clearly shows that it is necessary to apply intelligent trigger algorithms that take advantage of the non-uniform distribution of photons from neutrino interaction and thus limit the number of modules considered by the trigger.

For the diffusive ice, this will be basically impossible as the scattering will smear out the photon distribution while at the same time the long photon survival time requires trigger time windows of $t_{\mathrm{trig}} \gtrsim 2\,\mu\mathrm{s}$ to catch a major fraction of signal hits. Hence, low fake SN event rates in the diffusive ice can only be obtained at the cost of extremely low trigger efficiencies. For the clear ice in contrast, the event geometry (i.e. the distribution of light throughout the detector) is well preserved. In the following, we present two strategies that reject fake events induced by sensor noise. As these lead to reduction of the detection efficiency, we have extended the detector to a configuration with 127 strings in the same hexagonal geometry to retain the 10 Mton target set initially. This final geometry and the corresponding effective sensor density (in units of IceCube regular efficiency modules) are illustrated in Fig. 4 and will be used throughout the following.

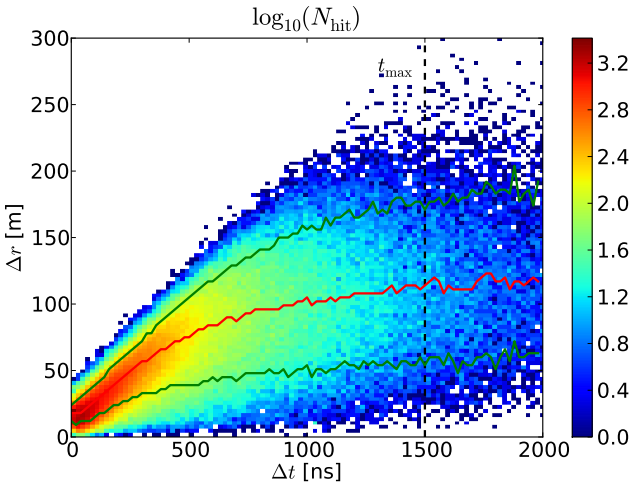

Figure 5: Distribution of signal hits in a simulated detector: spatial distance Δr to the vertex position vs. time difference Δt between the hit and the neutrino interaction.

4.1.1. Phase space cut

In case of a neutrino event, a positron from inverse beta decay produces Cherenkov light along its track, which is short compared to the scattering length in ice. These events are thus characterized by a localized emission of light. In contrast, events generated by random noise have no intrinsic topology and have hits distributed uniformly throughout the detector. The rate of noise events can thus be significantly reduced by only considering the part of the detector where a signal event would create most of the hits.

For this we define a fiducial volume within the detector that depends on the time and position of the neutrino vertex. As that vertex is not known a priori, we use a χ^2-minimization of the time residual of the photon propagation time minus the expected photon arrival time for straight propagation from the vertex to reconstruct the vertex position. Using this simple method, a positional resolution of $\sim 15\,\mathrm{m}$ can be achieved. To incorporate this limited knowledge of the vertex position, a random Gaussian smearing with 10 m standard deviation in each coordinate is applied to the vertex position of our simulated events. Fig. 5 shows the distribution of hits in the two-dimensional phase space given by the time between the hit and the neutrino interaction and the distance between the hit module and the reconstructed vertex. The 10% and 90% quantiles of the distance are calculated for this phase space (green lines in Fig. 5, red line is the median), giving the inner and outer radius of a spherical shell expanding with time and containing $\approx 80\%$ of the signal hits.

We now reassess the noise trigger rate by limiting the hits that contribute to an event to those within this phase space region (cf. Fig. 6) for all times up to t_{max}. As the phase space volume (i.e. the number of sensors that can

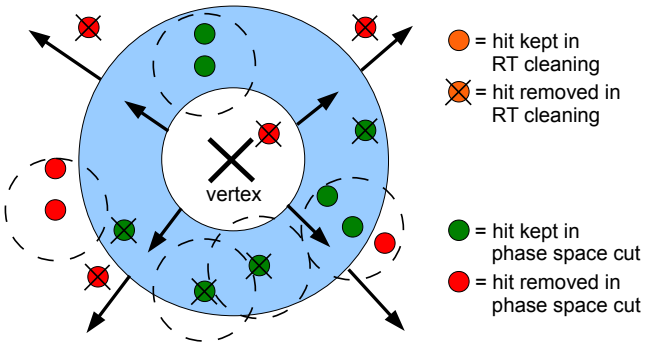

Figure 6: Illustration of the phase space cut and the local coincidence cleaning on a noise event. Each colored sphere corresponds to a hit optical module. The blue region indicates the expanding spherical shell used in the phase space cut, dashed circles indicate the radius of the local coincidence cleaning.

contribute to the trigger) quickly increases with t_{max}, the fake SN event rate f_{noise} is a strong function of t_{max} as well. We choose the value of t_{max} so that it limits $f_{\mathrm{noise}} \leq 1\,\mathrm{mHz}$ for a given sensor noise rate f_m, number of hits required to form a trigger n_{trig}, and the string spacing d_{str} of the detector and calculate the effective mass for SN signal neutrinos for each configuration.

We simulate the detector in the clear ice as described above with 127 strings of 300 m length (c.f. Fig. 4). Fig. 7 shows the resulting effective mass after this phase space cut is applied and Tab. 2 lists the optimal parameters as function of module noise f_m. While this method reduces the trigger efficiency for neutrino interaction by up to a factor of 10, at the same time the fake trigger rate is reduced by many orders of magnitude. For the module dark noise rate of 500 Hz provided by IceCube DOMs, achieving a fake trigger rate of 1 mHz is only possible at the cost

f_m [Hz]	M_{eff} [Mton]	d_{str} [m]	n_{trig}	t_{max} [ns]	$f^{\mathrm{PS}}_{\mathrm{noise}}$ [Hz]	f_{noise} [Hz]
10	7.51	25	5	590	$1 \cdot 10^{-3}$	1.0
50	3.77	15	7	430	$1 \cdot 10^{-3}$	3.4
500	1.18	15	9	250	$1 \cdot 10^{-3}$	$2.2 \cdot 10^{4}$

Table 2: Optimal parameters for string spacing (d_{str}), required hit multiplicity (n_{trig}) and maximum hit time window (t_{max}) together with resulting effective mass M_{eff} as function of module noise rate f_m. The parameters are chosen so that the phase space cut limits the rate of noise triggers to $f^{\mathrm{PS}}_{\mathrm{noise}} = 1\,\mathrm{mHz}$. The noise rates for the same configuration without the phase space cut are shown for comparison.

of simultaneously increasing the number of hits required for a trigger, decreasing the string spacing and using a short trigger time window. Due to these extreme choices, the trigger efficiency for neutrino events is low and the effective mass of this detector configuration falls short of the initial target of 10 Mton. In order to retain 10 Mton, reducing the sensor self-noise rate to $\sim 10\,\mathrm{Hz}$ per meter instrumented string is essential.

4.1.2. Local coincidence cleaning

While taking advantage of the localization of the event, the above method does not account for the fact that light from the positron is emitted in a preferred direction on the Cherenkov cone. As demonstrated for IceCube, requiring a local coincidence between photon hits is a very efficient way to reduce the effect of random noise [43]. A hit is required to be accompanied by at least another hit within a certain radius Δr and time window Δt in order to fulfill the local coincidence criterion. Fig. 6 shows an illustration of this process. We have applied such a radius-time cleaning to the simulated events and find it to provide additional background rejection power on top of the phase space cut. In order to optimize the parameters Δt and Δr, we apply the hit cleaning method to signal and noise events and then re-optimize the parameters of the phase space cut for the cleaned data set. The reduction of noise hits allows to increase t_{max} for the same f_{noise} of 1 mHz. Fig. 8 shows the effective mass obtainable with this additional cleaning for 10 Hz module noise to be increased by 60% from 7.5 Mton to 12 Mton.

4.1.3. Conclusion

Operation of a very dense detector at the lowest possible trigger threshold introduces a strong dependence of the trigger rate on the module noise. Algorithms exploiting the spatial and temporal distribution of the light (that can not be used in the diffusive ice) have to be employed to obtain a sufficiently low rate of fake events. While even more advanced algorithms considering the full event topology would still allow a moderate increase of the effective mass, this study demonstrates the importance of low-noise sensors. Correlated noise that was not treated here will be more difficult to reject and provides additional motivation to seek low dark noise rates in future photo-sensor R&D.

4.2. Muon background

Muons crossing the detector or passing nearby are easily separable from the SN neutrino signal via the huge amount of Cherenkov light produced by the extended track. An additional outer layer of the detector, naturally provided by IceCube in the deep clear ice, would ensure that even muons passing by at large distances or stopping just above the detector can be identified as such.

For a conservative first estimate of the effect of atmospheric muons, we assume all muons reaching the top of the detector being energetic enough to cross it. From [44]

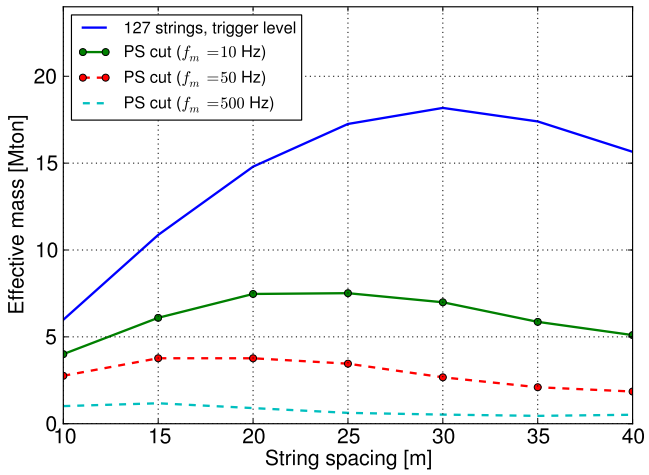

Figure 7: Effective mass of the simulated 127-string detector at trigger level (solid) and after a phase-space cut is applied to limit the fake trigger rate to 1 mHz for module noise rates of 500 Hz (dashed), 50 Hz (dashed, circles) and 10 Hz (solid, circles).

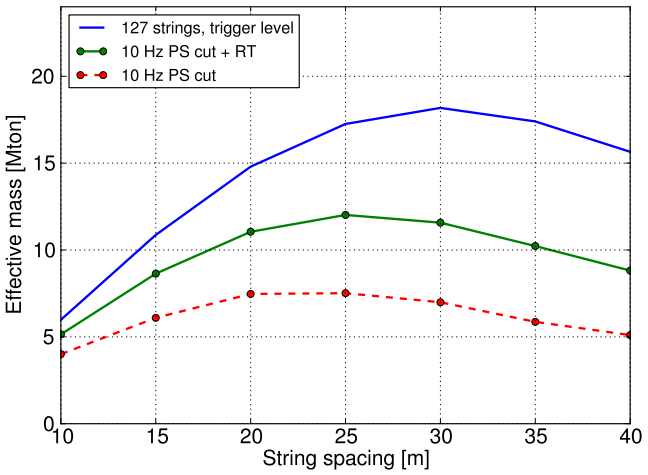

Figure 8: Effective mass of the simulated 127 strings detector with 10 Hz noise rate per module at trigger level (solid), with phase space cut applied (dashed, circles) and with phase space cut re-optimized after the radius-time cut is applied (solid, circles).

we obtain a muon flux of $\Phi_\mu = 8 \cdot 10^{-8}\,\mathrm{cm}^{-2}\mathrm{s}^{-1}\mathrm{sr}^{-1}$ for the top of the clear detector at 2150 m depth, giving a muon passing rate of about

$$R_\mu = \Phi_\mu \cdot 300\,\mathrm{m} \times 300\,\mathrm{m} \cdot \pi \approx 230\,\mathrm{Hz} \qquad (7)$$

using a detector cross-sectional area of $(300\,\mathrm{m})^2$ and an effective solid angle of π that accounts for the lower flux from angles closer to horizon where the ice shield is thicker. A muon traveling through the entire detector has a track length of $\approx 300\,\mathrm{m}$ and emits about $N_0 \approx 10^7$ Cherenkov photons on its path (≈ 360 photons per cm). We assume as a worst case that all photons are trapped within the detector volume by scattering to compute how long the photons will remain detectable within the detector before it is absorbed. The number of photons after a path $x = ct/n$ is given by:

$$N_\gamma = N_0 \cdot e^{-\frac{t}{t_{\mathrm{abs}}}}, \qquad (8)$$

with $t_{\mathrm{abs}} = n\lambda_a/c = 1.5 \cdot 10^{-6}\,\mathrm{s}$, for an absorption length of $\lambda_a \lesssim 100\,\mathrm{m}$ (as found in the clear ice) and a refractive index of $n = 1.31$. After a time

$$t = t_{\mathrm{abs}} \ln \frac{N_0}{N_\gamma} \approx 7\,\mu\mathrm{s} \qquad (9)$$

the number of unabsorbed photons in the detector due to a crossing muon has fallen below $N_\gamma = 1$ which is well below our trigger threshold. We therefore conservatively assume each passing muon to illuminate the detector for a time interval of $7\,\mu$s, which has to be accounted for as dead time for supernova neutrino detection, corresponding to a fraction of $R_\mu \cdot 7\,\mu\mathrm{s} = 0.16\%$ of detector operation time. A detector in the diffusive ice will not only experience a much higher muon passing rate of over 5000 Hz as it is located much closer to the surface. Because of the long absorption length of $\approx 350\,\mathrm{m}$, photons will remain in the detector for $\sim 25\,\mu$s, causing an effective dead time of $\approx 14\%$ during which the detector is saturated with photons.

These passing muons are easily identified because of the dense instrumentation and can be rejected applying a veto on down-going particle tracks. However, muons also produce spallation products by fragmenting ^{16}O nuclei [45]. The decay of these products mimics low-energy neutrino events and is a serious background. Super-Kamiokande has demonstrated [45, 46] that a cut on a likelihood function including spatial and temporal distance from the passing muon as well as energy loss of the muon can be used to efficiently remove spallation events. However this results in an additional 20% effective dead time for Super-Kamiokande which is located at a depth of 2700 meters water equivalent [45], comparable to the deep location considered here. For the shallow diffusive ice around 900 meters depth in contrast, spallation backgrounds may render neutrino detection entirely impossible.

4.3. Solar neutrino background

Put aside the cosmic neutrino background—which is too low in energy to be detectable—the by far dominant flux of neutrinos at the earth stems from the sun, where neutrinos are abundantly produced in several different fusion cycles [2]. As only ν_e and no $\bar{\nu}_e$ are generated in the sun, these solar neutrinos cannot undergo inverse beta-decay. The dominant interaction for solar neutrinos is elastic scattering on electrons. Interactions on oxygen nuclei are about two orders of magnitude less important [47] and are ignored here. Furthermore, only ^{8}B and hep neutrinos

need to be considered, since all other solar neutrino fluxes are below the detector's energy threshold at $\sim 1.7\,\mathrm{MeV}$. Since the flux of hep neutrinos is three orders of magnitude lower than the ^{8}B flux they are neglected here as well [48, 49].

To calculate the interaction rate, we use an analytical expression for neutrino-electron elastic scattering from Eqn. (5.25) in [2]

$$\frac{d\sigma}{dT_e}(E_\nu, T_e) = \frac{\sigma_0}{m_e}\left[g_1^2 + g_2^2\left(1 - \frac{T_e}{E_\nu}\right)^2 - g_1\, g_2\, \frac{m_e\, T_e}{E_\nu^2}\right] \quad (10)$$

with T_e being the kinetic energy of the recoil electron in the laboratory frame and

$$\sigma_0 = \frac{2\, G_F^2\, m_e^2}{\pi} \simeq 88.06 \cdot 10^{-46}\,\mathrm{cm}^2$$
$$g_1 = \frac{1}{2} + \sin^2\theta_W \simeq 0.73 \qquad g_2 = \sin^2\theta_W \simeq 0.23$$

and fold it with the energy-dependent effective mass of our detector given in Fig. 9(b). Taking the shape of the ^{8}B neutrino spectrum from [50] and normalizing it to a total flux of $\Phi(^8\mathrm{B}) \approx 2.44 \cdot 10^6\,\mathrm{cm}^{-2}\mathrm{s}^{-1}$ [47], we arrive at an approximate solar neutrino event rate of $\approx 75\,\mathrm{mHz}$ for a detector in the clear ice at trigger level. Additional application of the phase space cut (cf. Sec.4.1.1) and local coincidence cleaning (cf. Sec.4.1.2) reduces this rate to $\approx 28\,\mathrm{mHz}$, still significantly larger than the maximum allowed rate of random background events $f_{\max}^{\mathrm{BG}} = 1\,\mathrm{mHz}$.

However, a number of methods can be applied to further discriminate the rate of solar neutrino events. The bulk of solar neutrinos is less energetic than the bulk of SN neutrinos (cf. Fig. 9 (a)). Changing the trigger requirement from 5 hits to 7 hits increases the energy threshold and thus reduces the expected event rate of solar neutrinos by a factor of nearly four, while reducing the signal efficiency for SN neutrinos from the LL model by only 37%. Furthermore, the electron emerging from the elastic scatter roughly keeps the direction of the incident neutrino, while the inverse beta decay effectively randomizes the positron direction. For a sufficiently dense instrumented array such as Super-Kamiokande, an angular resolution of $\sim 30^\circ$ at $E_e = 10\,\mathrm{MeV}$ is feasible [46, 47]. Assuming a one-sigma (68% of the events) angular window of this size to reject neutrinos from the direction of the sun, we estimate to be able to further discriminate the solar neutrino rate to $f_\odot = (1 - 0.68)^3 \cdot 28\,\mathrm{mHz} \approx 1\,\mathrm{mHz}$, while retaining $(1 - (30^\circ)^2/\Omega_{sky})^3 \gtrsim 93\%$ of the SN events. The most powerful rejection will be achieved using a likelihood method that incorporates both the direction and energy for each event within the time window. In absence of a full reconstruction we refrain from a more detailed discussion, but note that the large rate of solar neutrinos can be significantly reduced. It is also worth mentioning that a fundamental prerequisite is the ability to reconstruct the direction of the emerging lepton, which can only be done in the clear ice where most photons are only slightly deflected before absorption. In the diffusive ice, all directional information is lost during the random walk of the photons.

events per 10 s	**solar ν_e**	**atm. $\nu_e + \bar{\nu}_e$**	**LL $\bar{\nu}_e$**
5 hits	0.753	0.0038	3.760
5 hits, PS+RT	0.282	0.0032	2.513
6 hits, PS+RT	0.158	0.0030	2.032
7 hits, PS+RT	0.079	0.0027	1.586

Table 3: Average number of events per 10 s from solar and atmospheric neutrino background (up to 100 MeV) as well as the SN neutrino signal for a LL supernova in 10 Mpc distance for different numbers of hit modules and with noise cleaning (PS+RT) applied.

4.4. Atmospheric neutrino background

Cosmic rays colliding with the Earth's atmosphere produce ν_e and $\bar{\nu}_e$ in similar abundance. The dominant component are the electron anti-neutrinos, interacting via inverse beta-decay with a cross-section two orders of magnitude higher than the neutrino-electron elastic scattering of electron neutrinos [46]. Taking the atmospheric neutrino flux calculations from [51], the neutrino-electron elastic scattering cross-section from Eqn. 10 and the cross-section for inverse beta-decay given in the phenomenological parametrization in [31] ("Naïve +" model) and integrating the event rate from $3 - 100\,\mathrm{MeV}$, we arrive at an expected trigger level event rate of $0.004\,\mathrm{mHz}$ for ν_e and $0.4\,\mathrm{mHz}$ for $\bar{\nu}_e$ triggering on 5 hit sensors in the clear ice. The resulting spectrum, also shown in Figure 9 (d), peaks well above the peak of SN interactions, allowing to further discriminate these events. While somewhat more abundant, elastic scattering of ν_μ is only possible via neutral current interactions, and thus has a factor six smaller cross-section.

Another component of the background are *invisible muons* that are produced by low-energy atmospheric muon neutrinos. These are muons below the threshold for Cherenkov light emission, that decay to an electron that has – due to its lower mass – a velocity above the Cherenkov threshold. These *Michel electrons* have been measured by Super-Kamiokande [46, 52] and amount to ~ 90 events per year in their effective volume of 22.5 ktons. Scaling this up to ~ 4000 events per Mton per year, we arrive at a corresponding rate of $\approx 1.5\,\mathrm{mHz}$ for a 12 Mton detector. While already small compared to the background of solar neutrinos, further reduction can be achieved by using the surrounding IceCube detector to veto accompanying atmospheric muons in the deep ice.

4.5. Summary

The large sensor multiplicity requires intelligent trigger and selection algorithms to cope with the backgrounds arising from sensor self-noise, atmospheric muons, solar as

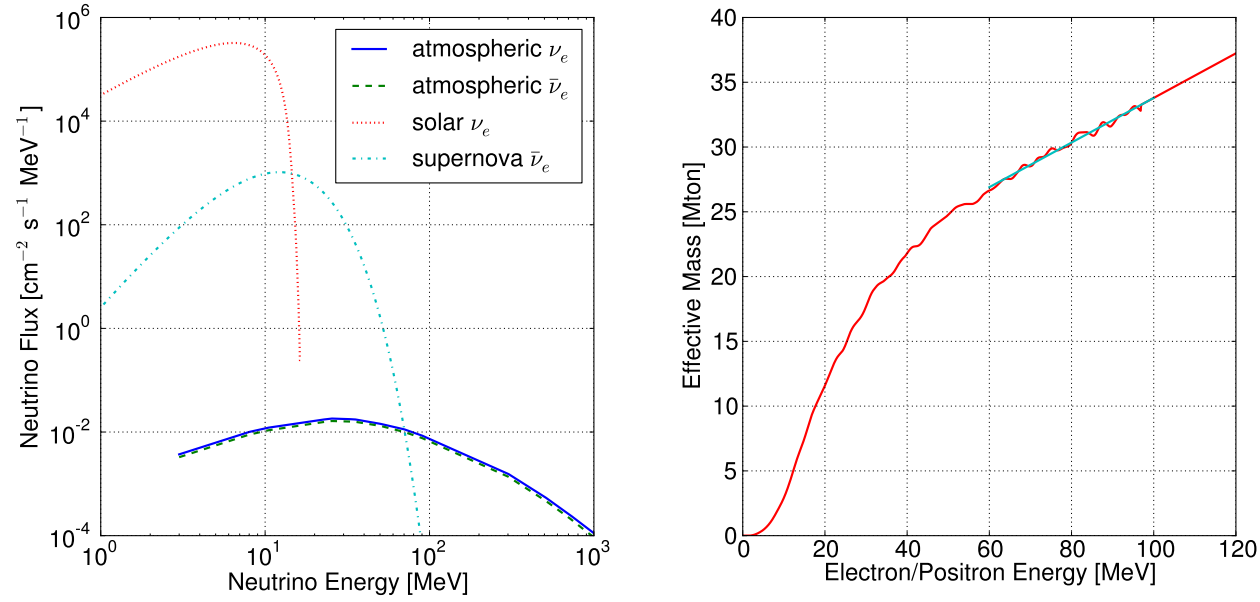

(a)

(b)

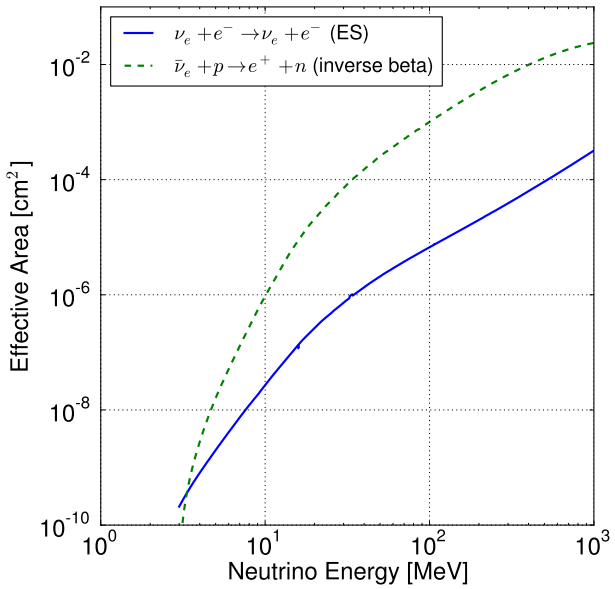

(c)

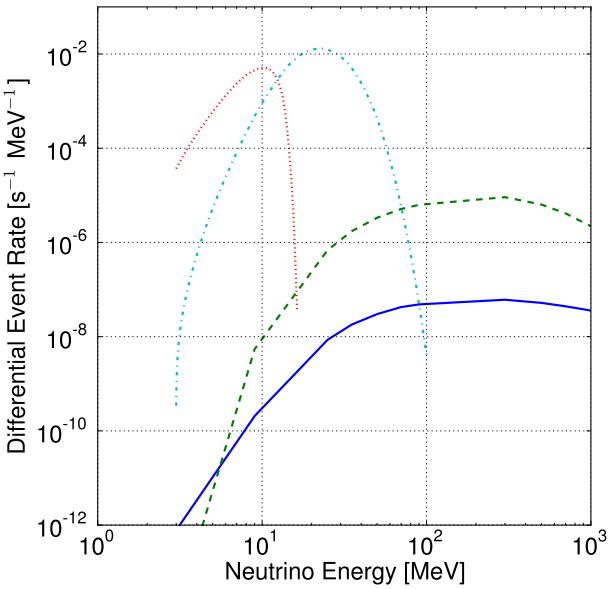

(d)

Figure 9: (a) The flux for solar [47, 50] and atmospheric [51] neutrinos as function of energy. The Supernova neutrino flux on Earth according to the LL model [26], normalized to an average power of $4.9 \cdot 10^{51}\,\mathrm{erg\,s^{-1}}$ in $\bar{\nu}_e$ for a supernova distance of 10 Mpc is shown assuming a burst duration of 10 s. (b) Effective mass as function of lepton energy for the 127-string detector in clear ice, triggering on 5 hit modules, after applying noise cleaning. Above 100 MeV, a linear extrapolation (dashed) is used. (c) The effective area for a 127-string detector for elastic scattering and inverse beta-decay. (d) Event rate per MeV as function of neutrino energy for solar, atmospheric and supernova neutrino fluxes from (a) with effective area from (c).

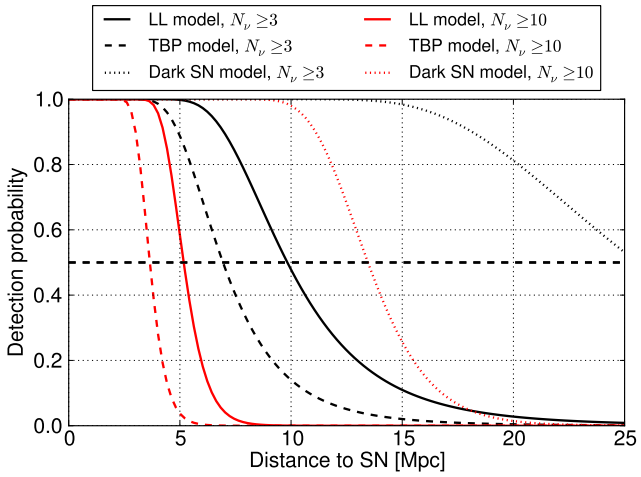

Figure 10: SN detection probability for the simulated 127 strings detector after application of noise cleaning as described in section 4.1. Shown are results for the LL model, the TBP model, and a dark supernova model (compare Table 1), for the detection of at least either 3 or 10 neutrino events from the SN.

well as atmospheric neutrinos. In this challenging background situation, a detector in the diffusive ice close to the surface is strongly disfavored due to a) the inability to reject self-noise triggers by their hit distribution pattern, b) the much higher muon background leading to significant downtime, c) the inability to use the surrounding IceCube and DeepCore detectors as muon veto and d) the solar neutrino backgrounds which cannot be vetoed effectively due to the lack of directional reconstruction. Even in clear ice, the suppression of noise to a sufficiently low level will be a major challenge and contingent on future improvements in sensor development. Due to the larger scattering length compared to the diffusive ice, the hit pattern is less localized, but contains directional information, making the application of event reconstruction both necessary and possible.

5. Expected supernova detection rate

Knowing the detector effective area as a function of neutrino energy (Figure 9 (c)), we can proceed to calculate the sensitivity to a supernova neutrino burst with a given spectrum. The probability to detect a supernova is calculated from Poisson statistics. We consider a supernova as detected if at least three neutrino events trigger the detector within 10 s, which is the threshold we can expect if all other backgrounds can be controlled to within 1 mHz. Figure 10 shows the SN detection probability as function of distance to the SN, using the three considered models, for the 127-string detector in the clear ice described in section 4.1 with noise cleaning applied. The distance up to which we will detect ≥ 3 neutrinos with a probability of $\geq 50\%$ is found to be 6.9 Mpc for the TBP model, 9.8 Mpc for the LL model and 25.6 Mpc for the dark SN model, respectively.

Galaxy	Type	SN Rate [SNu]
Elliptical	E-S0	< 0.05
Spiral-like	S0a-Sb	0.89 ± 0.33
Spiral	Sbc-Sd	1.68 ± 0.60
Others	Sm, Irr., Pec.	1.46 ± 0.71

Table 4: The expected rates of core-collapse supernovae for different galaxy types in supernova units ($1\,\mathrm{SNu} = 1\,\mathrm{SN}(100\,\mathrm{yr})^{-1}(10^{10}\,\mathrm{L}_\odot^\mathrm{B})^{-1}$). Values from [54], scaled by 1.68 (see text).

With this probability at hand along with the supernova rate in the local environment, we can compute the expected supernova detections. We start from a catalog of nearby galaxies that reaches up to 100 Mpc [53]. Following [54] we assume that the blue luminosity of a galaxy is proportional to the star formation rate and hence also to the supernova rate. The conversion factor will depend on the galaxy type and is obtained from SN observations (cf. Table 4). These conversion factors lead to a total SN rate that is lower by a factor 1.68 compared to a more recent result derived from a comprehensive compilation of local SNe [55]. We include this additional scale factor in our rate estimate to ensure consistency with currently available data. For a limited number of galaxies the catalog leaves the type unspecified. Testing the allowed range of conversion factors, this leads to an error $\leq 4\%$ on the total core-collapse SN rate for distances up to 20 Mpc.

Comparing with a theoretical prediction based on the initial mass function and cosmological star formation rate [9], our SN rate is still a factor two lower. One explanation might be that the conversion factors in Table 4 are based on observations with a bias to miss many faint SNe. Another possibility is a significant contribution of dark supernovae, that would not be detected optically, but still emit neutrinos [9]. Scaling our blue luminosity prediction by a factor of two, we also find good agreement with the observed rate of nearby SNe [56], and regard the rate estimates based on actual observations of SNe and those scaled to the star formation rate—both shown in Figure 11—as lower and upper limit, respectively.

Table 5 gives a summary of expected SN detections per decade in different neutrino event multiplicity bins. The total resulting number of SN detections for the simulated 127-string detector ranges from 23 to 46 per decade for the LL model and about half of that for the TBP model. For dark SNe we make the modest assumption that SNe collapse to a black hole at a rate of 10% of the regular core-collapse SN rate. Yet due to a more energetic neutrino spectrum, dark SNe are detected at a higher efficiency resulting in between 20 and 40 dark observations

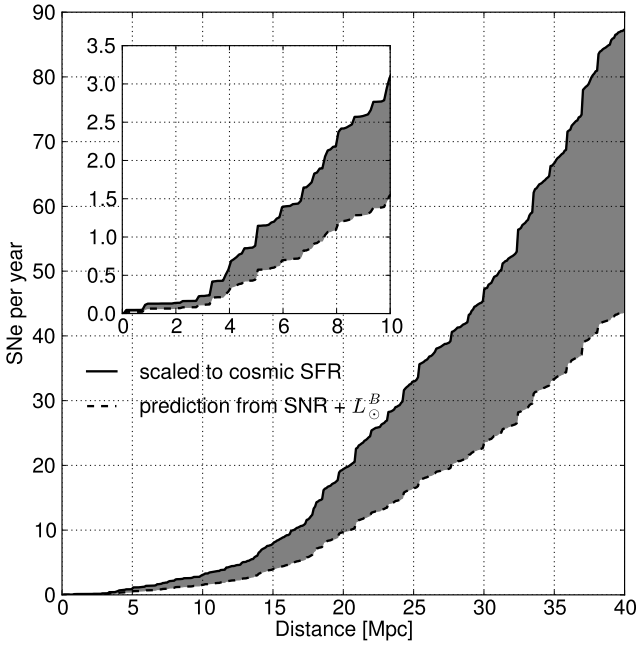

Figure 11: Range of cumulative expected supernova rate: lower curve (dashed) according to observed SN rate and blue luminosity [54], normalized to the results of [55], upper curve (solid) scaled by a factor 2 to match expectations from the cosmic star formation rate [9]. The galaxy distribution and their blue luminosity values are taken from [53].

per decade, comparable to the number of detections from the LL model. Altogether, one can expect to observe at least one SN per year on average, perhaps up to 5 or more. The rate of SNe producing strong bursts of ten or more neutrinos is between 0.3 and 0.6 per year without dark SNe, reaching up to ≈ 1 event per year if dark SNe are included. Remember that these numbers are obtained after applying the cuts to reject triggers from a sensor self-noise rate of 10 Hz as outlined in section 4.1. Cuts to fully reject the physical background of solar neutrinos are not yet included but we expect only a small reduction of rates from these.

6. Conclusion

A $\mathcal{O}(10)$ megaton scale neutrino detector is required to extend the sensitivity to core-collapse SNe beyond the Large Magellanic Cloud to neighboring galaxies and yield a detection rate of up to several SNe per year. In this paper we have explored two implementations for such a detector in the Antarctic ice: either in the diffusive ice (around 900 m below surface) where photon transport is diffusion dominated or in very clear ice (at around 2300 m depth) where photons can travel with very little scattering. In both cases, the detector geometry would resemble that of IceCube, however, with a much reduced string spacing and significantly increased density of photo-sensors per string.

number of neutrinos	**CCSNe (LL)**	**CCSNe (TBP)**	**Dark SNe**
3	8.7	3.6	5.9
4 - 5	5.6	2.8	6.5
6 - 9	3.6	2.3	4.5
$\geqslant 10$	5.5	2.6	3.4
sum $\geqslant 3$ ($\mathbf{L^B_\odot}$)	**23.4**	**11.3**	**20.3**
sum $\geqslant 3$ (SFR)	**46.7**	**22.7**	**40.5**

Table 5: Expected number of supernova detections within one decade by observed neutrino multiplicity based on per-galaxy rates from blue luminosity [54, 55]. The last lines show the sum of SN detections for this rate prediction ($L^B_\odot$), as well as for a prediction scaled to match the star formation rate (SFR) [9] (c.f. Figure 11). Dark SNe are assumed to occur at a fraction of 10% of all CCSNe.

To achieve the $\mathcal{O}(10)$ megaton scale with sensitivity to 10 MeV neutrinos at trigger level would require a 61-string installation with about 20,000 photo-sensors similar to the HQE sensors employed by IceCube for the diffusive ice location and about ten times that total photo-cathode area for the clear ice location.

Such a detector could be built in a similar manner as IceCube, by drilling holes into the ice and deploying strings holding the light sensors. However, with the demandingly large number of photo-sensors required, dedicated R&D for photo-sensors with large effective photo-cathode area seems appropriate. Besides the large effective area, we identify a low noise rate as crucial requirement for such a detector. Even for a self-noise rate of 10 Hz per meter instrumented string, the spatial and temporal distribution of hits has to be exploited and the number of strings increased to 127 to retain the $\mathcal{O}(10)$ megaton target effective mass. The short scattering length will render this method void for the diffusive ice, making the task to separate neutrino events from random noise triggers yet more difficult.

The main physical background remaining after the self-noise reduction arises due to solar ^{8}B neutrinos. Given a reconstruction algorithm, these can be identified via their angular proximity to the sun and lower photon multiplicity. Atmospheric muons will provide exceedingly bright events in such a dense installation, resulting in a small downtime for the deep ice. More challenging is the rejection of spallation events and Michel electrons, yet with the IceCube detector fully surrounding the array, their identification will be straight-forward and only a modest performance reduction will arise from their rejection.

Using a catalog of nearby galaxies, we have computed the rate of detectable SN neutrino bursts. We show that depending on the SN rate and explosion model assumed, we can expect to observe between 11 and 46 SNe per decade in neutrinos (not counting the dark SNe) in the 127 string detector configuration. By combining the ob-

servation of a neutrino burst with an optical detection of a SN, one can thereby disentangle the question of explosion model and SN rate. We note that in the future, with large, wide field optical surveys covering essentially the full sky, nearby SNe should be found in an even more systematic manner than today.

Dark supernovae, where the star collapses to a black hole, could produce more than 20 detectable bursts per decade. Such a SN can be indirectly identified through the absence of an optical counterpart (with the risk of confusing it with a regular, dust obscured SN), or more directly, by observing neutrinos of higher energies. The limited energy resolution of the detector ($\approx 30\%$ per neutrino event) should be sufficient to estimate the effective temperature of the neutrino emission and hence the origin of the burst.

A neutrino detector as described in this paper will not only yield a precise measurement of the local supernova rate and can uncover dark supernovae. A few of the supernovae will be closer, or perhaps even galactic, and hence yield a much higher number of coincident neutrinos, allowing to infer details about the explosion or even the neutrino hierarchy. Lastly we point out that the low energy threshold and very large effective mass make such a detector potentially interesting for a number of other physics phenomena, such as e.g. proton decay studies. While we have demonstrated that one can achieve the desired goal - routine observation of SNe in neutrinos - we acknowledge the assumptions we have made on our way. In particular, we have identified the development of large-area, low-noise photo-sensors suitable for deployment in the ice at South Pole as a key requirement.

Acknowledgements

We would like to thank Imre Bartos, John Beacom, Francis Halzen, Allen Hallgren and Lutz Köpke for fruitful discussions, as well as the IceCube collaboration for graciously allowing us to use its photon tracking software. We acknowledge support from the Helmholtz Alliance for Astroparticle Physics (HAP).

References

[1] W. Arnett, Supernova 1987A (1989). doi:10.1146/annurev.astro.27.1.629.

[2] C. Giunti, C. Kim, Fundamentals of neutrino physics and astrophysics, Oxford University Press, 2007.

[3] G. Raffelt, Supernova neutrino observations: What can we learn?, arXiv:astro-ph/0701677v2.

[4] A. S. Dighe, Physics potential of future supernova neutrino observations, arXiv:0809.2977v3.

[5] M. Ikeda, A. Takeda, Y. Fukuda, et al., Search for Supernova Neutrino Bursts at Super-Kamiokande, The Astrophysical Journal 669 (1) (2007) 519.

[6] R. Abbasi, Y. Abdou, T. Abu-Zayyad, et al., IceCube sensitivity for low-energy neutrinos from nearby supernovae, Astronomy & Astrophysics 535 (2011) A109. doi:10.1051/0004-6361/201117810.

[7] S. Ando, J. F. Beacom, H. Yüksel, Detection of Neutrinos from Supernovae in Nearby Galaxies, Phys. Rev. Lett. 95 (17) (2005) 171101. arXiv:astro-ph/0503321.

[8] M. D. Kistler, H. Yüksel, S. Ando, et al., Core-Collapse Astrophysics with a Five-Megaton Neutrino Detector, Phys. Rev. D83 (2011) 123008. arXiv:0810.1959.

[9] S. Horiuchi, J. F. Beacom, C. S. Kochanek, et al., The Cosmic Core-collapse Supernova Rate does not match the Massive-Star Formation Rate, Astrophys. J. 738 (2011) 154–169. arXiv:1102.1977.

[10] L. Yang, C. Lunardini, Revealing local failed supernovae with neutrino telescopes, Phys. Rev. D 84 (2011) 063002. arXiv:1103.4628.

[11] Y. Sekiguchi, K. Kiuchi, K. Kyutoku, et al., Gravitational waves and neutrino emission from the merger of binary neutron stars, arXiv:1105.2125.

[12] B. Dasgupta, T. Fischer, S. Horiuchi, M. Liebendorfer, A. Mirizzi, et al., Detecting the QCD phase transition in the next Galactic supernova neutrino burst, Phys.Rev. D81 (2010) 103005. arXiv:0912.2568.

[13] R. M. Humphreys, K. Davidson, The luminous blue variables: Astrophysical geysers, Publ. Astron. Soc. Pac. 106 (1994) 1025–1051. doi:10.1086/133478.

[14] S. Ando, K. Sato, Relic neutrino background from cosmological supernovae, New J. Phys. 6 (1) (2004) 170.

[15] G. Pagliaroli, F. Rossi-Torres, F. Vissani, Neutrino mass bound in the standard scenario for supernova electronic antineutrino emission, Astroparticle Physics 33 (5–6) (2010) 287–291.

[16] K. Nakamura, Hyper-Kamiokande: A next generation water Cherenkov detector, Int. J. Mod. Phys. A18 (2003) 4053–4063.

[17] K. Abe, T. Abe, H. Aihara, et al., Letter of Intent: The Hyper-Kamiokande Experiment — Detector Design and Physics Potential, arXiv:1109.3262.

[18] C. K. Jung, Feasibility of a next generation underground water Cherenkov detector: UNO, AIP Conf. Proc. 533 (2000) 29–34. arXiv:hep-ex/0005046.

[19] T. DeYoung, Neutrino Astronomy with IceCube, Mod. Phys. Lett. A24 (2009) 1543–1557. arXiv:astro-ph/0906.4530.

[20] L. Demirors, M. Ribordy, M. Salathe, Novel technique for supernova detection with IceCube, arXiv:1106.1937v2.

[21] D. J. Koskinen, IceCube – DeepCore – PINGU: Fundamental neutrino and dark matter physics at the South Pole, Mod. Phys. Lett. A26 (2011) 2899–2915.

[22] E. K. Akhmedov, S. Razzaque, A. Y. Smirnov, Mass hierarchy, 2-3 mixing and CP-phase with Huge Atmospheric Neutrino Detectors, arXiv:1205.7071.

[23] I. Bartos, A. Beloborodov, K. Hurley, S. Marka, Detection Prospects for GeV Neutrinos from Collisionally Heated Gamma-ray Bursts with IceCube/DeepCore, arXiv:1301.4232.

[24] K. Murase, K. Kashiyama, P. Meszaros, Subphotospheric Neutrinos from Gamma-Ray Bursts: The Role of Neutrons, arXiv:1301.4236.

[25] N. Schmitz, Neutrinophysik, 1st Edition, Teubner Studienbücher: Physik, Teubner, 1997.

[26] T. Totani, K. Sato, H. E. Dalhed, et al., Future Detection of Supernova Neutrino Burst and Explosion Mechanism, The Astrophysical Journal 496 (1) (1998) 216.

[27] T. A. Thompson, A. Burrows, P. A. Pinto, Shock Breakout in Core-Collapse Supernovae and its Neutrino Signature, The Astrophysical Journal 592 (2003) 434.

[28] H. T. Janka, Explosion Mechanisms of Core-Collapse Supernovae, arXiv:1206.2503.

[29] K. Nakazato, K. Sumiyoshi, H. Suzuki, et al., Oscillation and Future Detection of Failed Supernova Neutrinos from Black Hole Forming Collapse, Phys. Rev. D78 (2008) 083014. arXiv:0810.3734.

[30] K. Sumiyoshi, S. Yamada, H. Suzuki, S. Chiba, Neutrino signals from the formation of black hole: A probe of equation of state of dense matter, Phys.Rev.Lett. 97 (2006) 091101. arXiv:astro-ph/0608509.

[31] A. Strumia, F. Vissani, Precise quasielastic neutrino nucleon

cross section, Phys. Lett. B564 (2003) 42–54. arXiv:astro-ph/0302055.
[32] P. Askebjer, S. W. Barwick, L. Bergström, et al., Optical properties of deep ice at the South Pole: absorption, Appl. Opt. 36 (18) (1997) 4168–4180.
[33] M. Ackermann, et al., Optical properties of deep glacial ice at the South Pole, J. Geophys. Res. 111 (D13) (2006) D13203+.
[34] M. Aartsen, others (IceCube collaboration), Measurement of South Pole ice transparency with the IceCube LED calibration system, Nucl.Instrum.Meth. A711 (0) (2013) 73 – 89.
[35] E. Andres, P. Askebjer, S. Barwick, et al., The AMANDA neutrino telescope: principle of operation and first results, Astroparticle Physics 13 (1) (2000) 1–20.
[36] R. A. Porrata, The Energy Spectrum of Pointlike Events in AMANDA-A, PhD dissertation, University of California (1997).
[37] J. Lundberg, P. Miocinovic, K. Woschnagg, et al., Light tracking through ice and water – Scattering and absorption in heterogeneous media with Photonics, Nucl.Instrum.Meth. A581 (3) (2007) 619 – 631. arXiv:astro-ph/0702108.
[38] K. Woschnagg, Photonics Web Page.
URL http://icecube.berkeley.edu/kurt/photonics/
[39] A. Olivas, D. Chirkin, K. Hoshina, et al., Photonics at sourceforge.net.
URL http://photonics.sourceforge.net
[40] R. Abbasi, et al., The IceCube Data Acquisition System: Signal Capture, Digitization, and Timestamping, Nucl.Instrum.Meth. A601 (2009) 294–316. arXiv:0810.4930.
[41] R. Abbasi, et al., Calibration and Characterization of the IceCube Photomultiplier Tube, Nucl.Instrum.Meth. A618 (2010) 139–152. arXiv:1002.2442.
[42] S. Böser, M. Kowalski, L. Köpke, L. Schulte, M. Voge, A Single Photon Sensor employing Wavelength-shifting and Light-guiding Technology, in preparation.
[43] J. Ahrens, J. Bahcall, X. Bai, et al., Sensitivity of the IceCube detector to astrophysical sources of high energy muon neutrinos, Astroparticle Physics 20 (5) (2004) 507 – 532.
[44] E. V. Bugaev, et al., Atmospheric muon flux at sea level, underground and underwater, Phys. Rev. D58 (1998) 054001. arXiv:hep-ph/9803488.
[45] Y. Fukuda, et al., Measurements of the solar neutrino flux from Super-Kamiokande's first 300 days, Phys. Rev. Lett. 81 (1998) 1158–1162. arXiv:hep-ex/9805021.
[46] M. Malek, M. Morii, S. Fukuda, et al., Search for Supernova Relic Neutrinos at Super-Kamiokande, Phys. Rev. Lett. 90 (2003) 061101.
[47] W. Haxton, R. Robertson, Solar neutrino interactions with O-18 in Super-Kamiokande, Phys. Rev. C59 (1999) 515–519. arXiv:nucl-th/9806081.
[48] J. N. Bahcall, C. Pena-Garay, Solar models and solar neutrino oscillations, New J. Phys. 6 (2004) 63. arXiv:hep-ph/0404061.
[49] J. N. Bahcall, A. M. Serenelli, S. Basu, New solar opacities, abundances, helioseismology, and neutrino fluxes, Astrophys. J. 621 (2005) L85–L88. arXiv:astro-ph/0412440.
[50] J. N. Bahcall, E. Lisi, D. E. Alburger, et al., Standard neutrino spectrum from ^{8}B decay, Phys. Rev. C 54 (1996) 411–422.
[51] T. Gaisser, T. Stanev, G. Barr, Cosmic Ray Neutrinos in the Atmosphere, Phys. Rev. D38 (1988) 85.
[52] J. F. Beacom, The Diffuse Supernova Neutrino Background, Ann.Rev.Nucl.Part.Sci. 60 (2010) 439–462. arXiv:1004.3311.
[53] D. J. White, E. J. Daw, V. S. Dhillon, A List of Galaxies for Gravitational Wave Searches, Class.Quant.Grav. 28 (8) (2011) 085016. arXiv:1103.0695.
[54] E. Cappellaro, R. Evans, M. Turatto, A new determination of supernova rates and a comparison with indicators for galactic star formation, Astronomy & Astrophysics 351 (1999) 459. arXiv:astro-ph/9904225.
[55] W. Li, R. Chornock, J. Leaman, et al., Nearby supernova rates from the Lick Observatory Supernova Search - III. The rate-size relation, and the rates as a function of galaxy Hubble type and colour, Mon. Not. R. Astron. Soc. 412 (2010) 1473–1507. arXiv:1006.4613.
[56] S. Horiuchi, J. F. Beacom, M. S. Bothwell, T. A. Thompson, Effects of stellar rotation on star formation rates and comparison to core-collapse supernova rates, arXiv:1302.0287.